Iraqi Geological Journal *Petros and Karo* *2023, 56 (2B), 278-301*

Iraqi Geological Journal

Journal homepage: https://www.igj-iraq.org

Petrogenesis of Amphibolite/Hornblendite Dikes in Qala-Diza Area, Iraqi Kurdistan Region

Jolyana R. Petros[1,*] and Nihad M. Karo[2]

[1] Department of Applied Geosciences, College of Spatial Planning and Applied Science, Duhok University, Duhok, Iraq

[2] Department of Earth Science and Petroleum, College of Science, Salahaddin University, Erbil, Iraq

* **Correspondence**: Joleanaramzi996@hotmail.com

Received:
20 November 2022

Accepted:
20 March 2023

Published:
31 August 2023

Abstract

The amphibolite and hornblendite dikes occur as part of the igneous complexes of Bulfat Ophiolite within the Zagros Suture Zone, NE Iraq. The igneous complex is part of the upper allochthonous ophiolite terrane within the second unit of the Penjween-Walash Subzone. This article discusses the petrogenetic characteristics and tectonic setting of the amphibolite rocks based on their petrography, mineral chemistry, and whole-rock geochemistry. Petrographically, both banded and massive amphibolites reveal that the main mineral constituents are amphibole and plagioclase with accessory clinopyroxene, opaques, sphene, apatite, rutile, zircon, sericite, epidote and chlorite; meanwhile the hornblendites consist of >90% amphibole with minor amounts of pyroxene, opaques, plagioclase, titanite, quartz, apatite, zircon, and chlorite. The amphibolites are divided into two types, banded (foliated) and massive, (non-foliated). The dominat textures of amphibolites are porphyroblastic, granoblastic, poikiloblastic, nematoblastic, and blasto-ophitic; meanwhile those of hornblendites are equigranular, poikilitic, cataclastic, and intergranular. The electron microprobe analysis (EPMA) showed that the amphiboles of the banded amphibolite range between tschermakite, magnesio-hornblende and pargasite; and those of the massive amphibolites range between magnesio-hornblende and actinolite; meanwhile those of hornblendites are dominantly tschermakite with minor magnesio-hornblende and pargasite. The plagioclase of the banded amphibolites is mainly oligoclase and andesine; and those of the massive amphibolites are mostly anorthite. Chemical classification diagrams indicated that the studied rocks are had low alkalies (Na2O+K2O), tholeiitic, ultrabasic to basic, alkaline to subalkaline and divided between foidite, picrobasalt and basalt. Various tectonic discriminating diagrams showed that most of studied rocks are mid-ocean ridge basalt (MORB). The studied amphibolites have been subjected to amphibolite facies metamorphism.

Keywords: Amphibolite; Hornblendite; Petrography, Petrogenesis; Bulfat Ophiolite; Iraqi Kurdistan Region

1. Introduction

Amphibolite rocks are the most common mafic metamorphic rocks, consisting dominantly of amphibole and plagioclase (Frisch et al., 2010; Gill and Fitton, 2022). These rocks can be formed by metamorphic process of the magnesium- and iron-rich igneous rocks; such as basalt and gabbro during regional metamorphism under high temperature and high pressure conditions (Wilson, 2020). Most

DOI: 10.46717/igj.56.2B.22ms-2023-8-31

amphibolite rocks have a distinctive lineation produced by the alignment of elongate crystals of amphibole. Some amphibolites are foliated because of the abundance of platy minerals like amphibole if platy minerals like mica, meanwhile the massive amphibolites are mostly non-foliated (Christiansen and Hamblin, 2014). Amphibolites have been studied in many geologic settings in many courtiers including Tomar Cordoba Shear Zone in Portugal (De Oliveira et al., 2003), Nigde metamorphics in Turkey (Kocak et al., 2007), ophiolitic me´langes along Bangong-Nujiang suture in Central Tibet (Wang et al., 2008), Penjween ophiolite in Iraq (Hadi, 2013). Neoproterozoic subduction along the Ailaoshan zone in China (Cai et al., 2014), Nagaland ophiolite complex in India (Bhowmik and Ao, 2016), Loch Maree Group in Scotland (Drummond et al., 2020), and Sanandaj-Sirjan zone in Iran (Sadegh et al., 2021).

Hornblendites are ultramafic magmatic rocks dominated by amphibole (Polat et al., 2012), and are commonly associated with other igneous and metamorphic rocks (Kettanah et al., 2021). These rocks are formed by settling of early crystallized amphiboles in hydrous magmas (Daczko et al., 2016). They form in many geologic settings and have been studied in Ivrea zone in Italy (Abart et al., 2001), Rio Negro complex in Brazil (Mendes et al., 2004), Fiskenæsset layered anorthosite complex in Greenland (Polat et al., 2012), Guyang hornblendite complex. In China (Ma et al 2016), Wang Nam Khiao area in Thailand (Fanka et al., 2016), Naein Ophiolite in Iran (Torabi et al., 2017), Alpine-Carpathian-Pannonian (ALCAPA) terrain in Hungary et al., (Bali et al., 2018), Central Andean arc magmatic systems Bolivia (Santana et al., 2020) and Penjween ophiolite in Iraq (Kettanah et al., 2021).

The Bulfat Igneous Complex forms the major part of the Bulfat Ophiolite which consists of large variety of intrusive igneous rocks including hornblendite, pyroxenite, hornblende gabbro, olivine gabbro, diorite, gabbro-diorite, syenite and granite with a crystallization age ranging between ~40 and ~ 45Ma (Aswad et al., 2013; Ali., 2017). These intrusions are hosted by the Gimo-Qandil Sequence (Albian-Cenomanian) which consists of calcsilicates, carbonates, metapelites, and metavolcanic rocks; and have been influenced by low to medium grade of regional metamorphism (Jassim et al., 1982 b; Karo, 2015) corresponding to the greenschist facies or to the onset of the amphibolite facies (Jassim et al., 1982a; Jassim et al., 2006). Serpentinites of the Bulfat area occur along the base of the nappe, and in an isolated peridotite body near Pouza (Jassim et al., 2006).

This article is focusing on amphibolite and hornblendite intrusions. The studied bodies have been collected from several traverses in five localities southeast of Qala-Dizah city and close to the Iraqi-Iranian border. The aim of this research is to study the petrogenetic characteristics and tectonic setting of the investigated area based on the petrography, mineral chemistry, and whole-rock geochemistry for amphibolite and hornblendite dikes hosted by serpentinite and metacarbonates of Bulfat area.

2. Geologic and Tectonic Setting

Iraq forms the northeastern part of the Arabian plate which is tectonically controlled by the collision between the Iranian and Arabian plates (Fouad, 2015; Abdulnaby, 2019). The collision between these plates started during the lower Tertiary and is still going on which resulted in the formation of the foreland basin and the Zagros-Taurus Mountain belt (Mohajjel et al., 2003; Al-Qayim et al., 2012; Al humadi et al., 2019). According to Jassim and Buday (2006), Iraq is tectonically divided into three parts: (1) Stable Shelf which is subdivided into Salman, Mesopotamia, and Rutba- Jezira zones; (2) Unstable Shelf which is divided into Imbricated, High Folded and Foothill zones; and (3) Zagros Suture Zone (ZSZ) which is divided from southwest to northeast into the following three zones:

- The Qulqula- Khwakurk Zone: The Qulqula Group consists mostly of Cretaceous radiolarian chert and limestone with imbricates of Permian, Triassic and Jurassic limestone. The Khwakurk Group consists of chert, volcanic and ultramafic rocks of the southern Neotethys (Jassim and Goff, 2006).

- 2The Penjween-Walash Zone which includes three Cretaceous intrusive complexes like Pushtashan, Mawat and Penjween as well as Paleogene Bulfat complex and the Cretaceous sedimentary and metamorphosed volcanic rocks, and unmetamorphosed Paleogene volcanic arc with mafic intrusions. These units were formed during the closure of the Neotethyan Ocean.
- The Shalair Zone is composed of thrust sheets of metamorphosed pelitic rocks (mostly phyllites) of Shalair Group, Cretaceous volcanic arc, and meta-carbonates of Mesozoic age.

Bulfat area is one of the disconnected fragments of oceanic lithosphere exposed at Jabal Bulfat in Zagros region, about 30 km east of Qala Dizah City, NE Iraq (Ali et al., 2012; Ali., 2017). It comprises volcano-sedimentary sequence of Gimo-Qandil Group (Jassim et al., 2006; Aswad et al., 2011) which originally named Bulfat Group (Jassim et al., 1987a; Karo, 2015). The Gimo group of Bulfat area includes regionally metamorphosed volcanics and volcano-sedimentary sequence (Jassim et al., 1982b), later it was intruded by igneous intrusion of Bulfat Complex (Buda, 1993). These intrusions mainly comprise pyroxene-hornblende and gabbros-diorite which are considered older intrusion intruded by younger olivine gabbro-diorites (Jassim et al., 2006a); as well as syenite and nepheline syenite formed during the late stage of the magmatic differentiation (Jassim et al., 2006a; Aswad et al., 2016).

Ultramafic igneous rocks in this area occur in the lower parts of complex, and can be divided into three occurrences like serpentinites, pyroxenites, and Pauza ultramafic body (Buday and Jassim, 1987). Ultramafic rocks of the Pauza Village are represented by peridotite affected by the serpentinization process, and forms 4% of the Bulfat ophiolite (Hamasalh, 2004). Discontinuous imbricated serpentinite occurs along the thrust zone between Halsho and Hero villages, separating the Eocene-Oligocene Walash-Naopurdan volcanic-sedimentary arc rocks from the metavolcano-sedimentary units of Gimo-Qandil Group (Albian-Cenomanian) (Jassim et al., 2006; Karo, 2015). The geologic map of the Bulfat area and locations of the studied samples are shown in Fig. 1. Amphibolite and hornblendite rocks appeared in the area as dykes in contact with the other rocks mainly serpentinized and metacarbonates as host. It occurs in various forms ranging from massive bodies to banded.

3. Methodology and Field Description

Based on the field observations, amphibolite rocks are divided into banded and massive types. The studied rocks are mostly characterized by extremely heterogeneous grain size that occurs as dikes cutting host rocks which are mostly serpentinites with the exception of metacarbonates of Gere traverse (Fig. 2A). Banded amphibolite is marked by the foliation as a result of alternating segregated dark-coloured amphibole and light-coloured bands (Fig. 2B). Meanwhile, massive amphibolite is characterized by granoblastic texture with their main minerals (amphiboles and plagioclase) which are mixed and not affected by banding. The hornblendites are black and medium- to fine-grained in hand specimens (Figs. 2C & 2D). These rocks occur as intrusions and dikes (Fig. 2C) cutting serpentinite host rocks; some samples are not collected from outcrops on the hill due to the presence of mine. therefore, the samples were collected under the hill (Fig. 2D).

More than 50 samples of amphibolite and hornblendite have been collected from five various localities (Fig.1). In total 48 thin sections have been prepared, twenty-four from the banded amphibolite samples, seven from the massive amphibolites, and seventeen thin sections from the hornblendite samples.

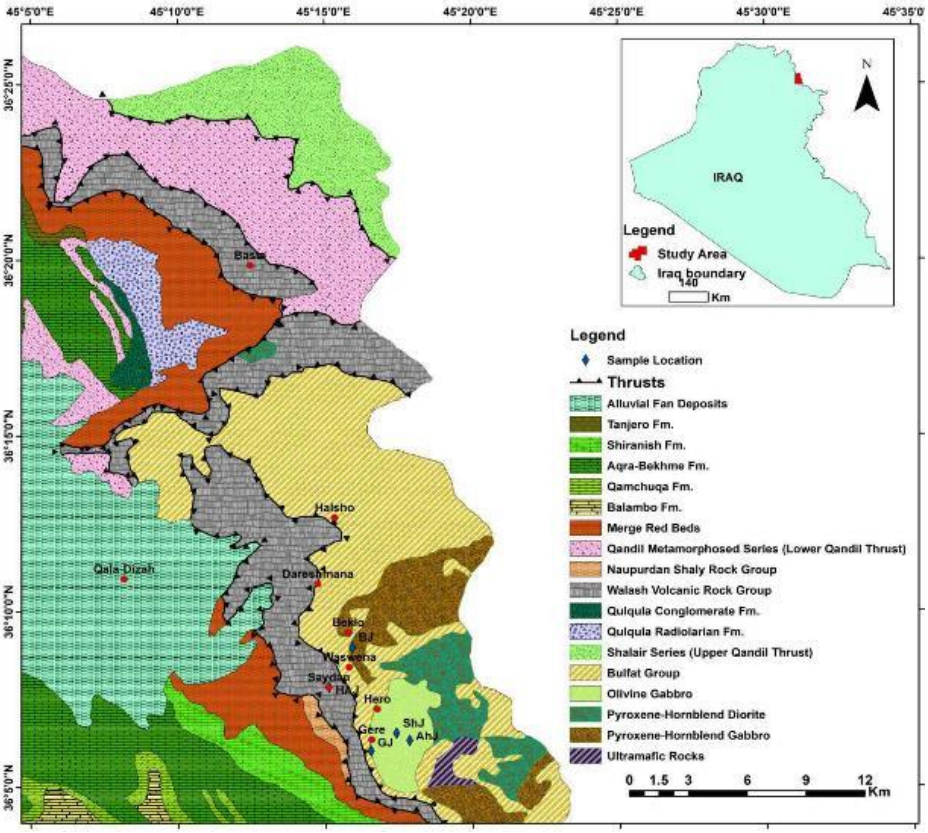


Fig.1. Geological map of Bulfat area showing the locations of the studied rock samples (Buda, 1993)**.**



Fig. 2. Field photographs of the studied amphibolite and hornblendite dikes: (A) Amphibolite intrusion cutting metacarbonates host rock; (B) The banded amphibolites with distinct lineation; (C) Hornblendite dike within one of the hornblendite outcrops; (D) Hornblendite dikes.

Many hornblendite samples were taken long traverse called "Sh" lies 2 km northwest of Hero village. Six banded amphibolite samples were collected long "BJ" traverse lies 3.7 km southeast of Darishmana village. Two banded amphibolite samples, one massive amphibolite sample, and one hornblendite sample were collected from south of Hero village along the traverse called "GJ". Many

hornblendite samples were taken along "HAJ" traverse which located 1.41 km northwest of Hero village. Five samples of massive amphibolite rocks were collected along "AhJ" traverse, located 2.41 km southeast of Hero.

These thin sections were examined in detail by polarized microscope for the identification of minerals and textures, and also to illustrate the effects of deformation and alteration/metamorphism on the studied rocks. The minerals percentage in studied samples are determined by using point counter method. Chemical compositions of minerals determined at Charles University in Prague with electron microprobe technique (EPMA) using a FEG-EPMA JXA-8530F (Jeol) microprobe under operating conditions of 15 kV accelerating potential and 20 nA beam current and the ZAF online program was used for data correction. Albite (Na), Corundum (Al), Apatite (P), Tugtupite (Cl), Diopside (Ca), Sanidine (K), Rutile (Ti), Chromium _Oxide (Cr), Barite (Ba), Vanadium (V), Magnetite (Fe), Rhodonite (Mn), Sphalerite (Zn), Ni (Ni), F-Topaz (F), Quartz (Si), and MgO (Mg) standards were used to measure elements indicated in brackets.

Whole-rock geochemistry (major and trace elements including the rare earth elements (REE) and loss-on-ignition were analyzed at ALS Laboratory Group in Seville, Spain using ICP-MS, ICP-AES, WST-SEQ with the Lithium Borate fusion method as a whole rock package encoding (ME-ICP06), (ME-MS 81D), (OA-GRA05) and (TOT-ICP06). The major elements were determined by ICP-MS (ME-ICP-06). Trace and REE elements were determined by ICP-MS ME-MS 81^{TM} plus method. Base metal reported with ME-MS 81 method by 4-acid digestion. Only available as an add on to ME-MS 81.

4. Results

4.1. Petrography

Forty eight thin sections were examined in detail by polarized microscope for the identification of minerals and textures and also to show the effects of deformation and alteration and/or low-grade metamorphism on the studied rocks. Petrographically, both banded and massive amphibolites reveal that the main mineral constituents are amphibole and plagioclase; whereas, hornblendites contain >90% amphiboles. These rocks were affected by various degrees of alteration which resulted in the formation of secondary minerals such as chlorite, sericite, and epidote. These alterations resulted in changes of the original characteristics of the primary minerals such as veining. Both banded and massive amphibolite thin sections have granoblastic and porphyroblastic textures; whereas, the main textures displayed by hornblendites are equigranular, poikilitic, cataclastic, and intergranular. The description of these rocks is given below.

4.1.1. Banded amphibolite

Banded amphibolites mainly consist of hornblende (50-70 %), and + plagioclase (10-40 %), with minor mounts of ± cliopyroxene (2-7 %), + opaque minerals (3-7%), + sphene (2-5 %), ± biotite (2 %), ± apatite (<1 %), ± rutile (<1 %), ± zircon (<1 %), ± zeolite (<1 %), ± sericite (<5%), ± chlorite (<2 %), and ± epidote (<1 %). In most thin sections, the foliation of banded amphibolites is reflected as segregated alternating bands of dark-coloured amphibole and light-coloured plagioclase.

Green-coloured amphibole is the most abundant mineral in banded amphibolites (Fig. 3A) which show distinct pleochrois from yellow to green, and high relief. It is mostly anhedral-shaped of variable sizes ranging from coarse-grained (8mm) to fine grained (<1mm) with oxidation products along the cleavage traces and grains boundaries (Fig. 3A). Hornblende grains occurs as phenocrysts or tiny crystals in the groundmass and also as euhedral inclusion in secondary amphibole (Fig. 3A). Phenocrysts of amphibole contain small inclusions of plagioclase, opaque minerals, apatite, rutile, and zircon (Fig. 3B). The extinction angle of prismatic shaped crystals range from 14° to 25°. Most prismatic crystals

are oriented along the foliation direction of these rocks (Figs. 3B, D). Some grains show zoning due to the change of the composition from the core toward the rim indicating that the equilibrium conditions were not achieved (Downes et al., 2004), as well as undulose extinction, and are commonly twined.

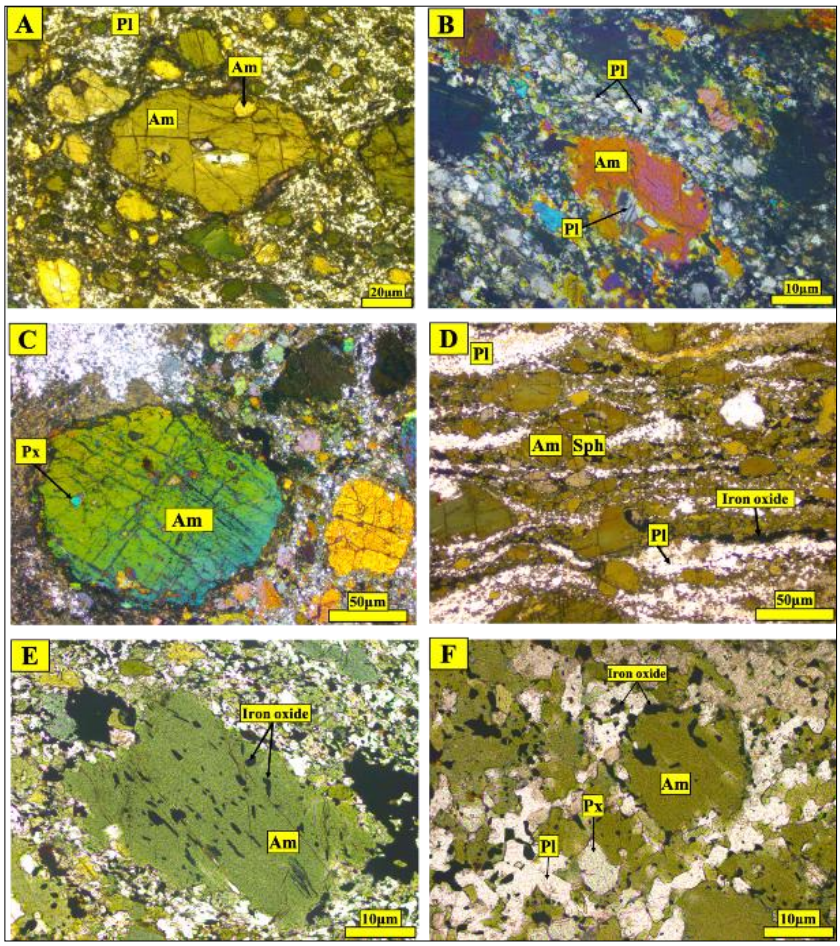


Fig. 3. Photomicrographs of the amphibolite rocks: (A) large unhedral crystal of amphibole surrounded by fine crystals of amphibole and plagioclase (plain polarized light: PPL); (B) Plagioclase enclosed by amphibole (XPL); (C) Amphibole grain encloses tiny inclusion of relic pyroxene (crossed polarized light: XPL); (D) Small grains of opaque mineral along amphibole and sphene boundaries oriented like band along the rock foliation (PPL); (E) Amphibole crystal contains numerous, oriented, small opaque inclusions (PPL); (F) Opaque mineral as small grains around amphibole grains and as inclusion within amphibole grains in massive amphibolite (PPL). Am = Amphibole; Pl = Plagioclase; Px = Pyroxene; Sph = Sphene; Bt = Biotite; Zr = Zircon; PPL = plainpolarized light; XPL = crossed polarized light.

Plagioclase minerals are mostly fine-grained and appear mainly in groundmass, with subhedral or anhedral crystal habits and granular or elongate shape (Fig. 3B). Unlike the fine-grained crystal, most of the coarse-grained plagioclase grains show polysynthetic twining (Fig. 3B). Alteration of some plagioclase grains resulted in their partial to pervasive sericitization and/or epidotization. Plagioclase shows blasto-ophitic and blasto-subophitic textures where anhedral and subhedral crystals of plagioclase are completely or partially enclosed by the secondary amphiboles (Fig. 3B).

Some of the thin sections from the banded amphibolites show deformation where plagioclase displays undulose extinction and deformed twins. Pyroxene grains have mainly anhedral to subhedral habits, and form about 2–8% of the total volume of the rocks. The pyroxene grains are mostly altered to secondary amphibole and the relict pyroxene appear as inclusions within amphibole (Fig. 3C). Opaque minerals range in shape from anhedral to euhedral, occur as elongate, irregular and rhombic crystals

along amphibole grain boundaries (Fig. 3D). The cores of some hornblende grains contain numerous, oriented, tiny opaques inclusions aligned along cleavage planes (Fig. 3E). According to backscattered image (BSE) of EPMA, Ilmenite also appears as an inclusion within amphibole (Fig. 5A). Ilmenite is sometimes surrounded by sphene (Fig. 5B), indicating that they have formed from it by alteration (Buda, 1993).

Occurrence of magnetite along amphibole boundaries (Fig. 5B) which are possibly related to metamorphic reactions and recrystallization (Polat et al., 2012). Rutile which is not common, occurs as inclusions within hornblende, sphene, and ilmenite. It is mostly produced from the alteration of other titaniferous minerals like Ilmenite and sphene (Demange, 2012).

Sphene is a common accessory mineral characterized by euhedral to anhedral crystal habit, very high relief, and pale brown colour (Fig. 3D). It occurs as small grains or as inclusion in amphibole. Sphene presence indicates high temperature condition (Hassan and Ridha, 2018). Apatite occurs as tiny six sided inclusion in amphibole and as grains in groundmass (Fig. 5A). Chlorite which is not common; has flaky shape, pale green colour and lacks pleochroism, and mainly found as retrograde chloritization alteration product (Fig. 5A). Biotite is not common, occurs as grains in the matrix or as inclusions in amphibole (Fig. 5B).

4.1.2. Massive amphibolite

The massive amphibolites mainly consist of + amphibole (50%-80%), + plagioclase (10%) with minor amounts of ± pyroxene (5%), ± apatite, ± opaque minerals (<5 %), ± rutile (<1 %); and some secondary minerals such as ± sericite (<1 %), ± epidote (<1 %) and ± chlorite (<1 %). Scapolite occurs in veins in some samples. The main textures encountered between amphibole and plagiocalse within the massive amphibolite are granublastic, porphyroblastiv, nematoblastic, poikiloblastic, blasto-ophitic texture.

The green-coloured amphibole crystals are anhedral to subhedral, granublastic, coarse- (8mm) to fine-grained (<1 mm) (Fig. 3F). Many crystals show Carlsbad twinning. The extinction angles of hornblende crystals range between 12° to 20°. Basal sections are characterized by symmetrical extinction. Amphibole in some thin sections is brown-coloured, prismatic in shape and anhedral in habit with parallel extinction. Poikiloblastic amphiboles contain opaques, plagioclase, biotite, rutile, apatite, and, zircon inclusions (Fig. 4A). Some amphibole crystals show chloritization. The brown amphibole is distinguished by its high iron content (Demange, 2012).

Plagioclase grains are mostly fine-grained, euhedral to anhedral in shape, or granular in within the groundmass (Fig. 3F). Based on extinction angle, some crystals are Na-rich (albite); meanwhile, the results of EPMA analysis also indicate the existence of anorthite. Large plagioclase grains show polysynthetic twinning which is lacking in the small-sized grains (Fig. 4B). Some crystals are replaced by sericite and minor epidote. Plagioclase displays undulose extinction and deformation twins. Blasto-Ophitic and sub- ophitic texture is also observed when a relatively individual crystal of plagioclase is completely enclosed by relic pyroxene or amphibole crystal (Figs. 4A & 4B). Pyroxene has anhedral to subhedral habits, and medium- to fine-grained (Figs. 3F & 4B). It is mostly diopside in the composition according to extinction angle. Proxenes are mostly altered to amphibole indicated by the presence of their remnants as inclusions within amphibole.

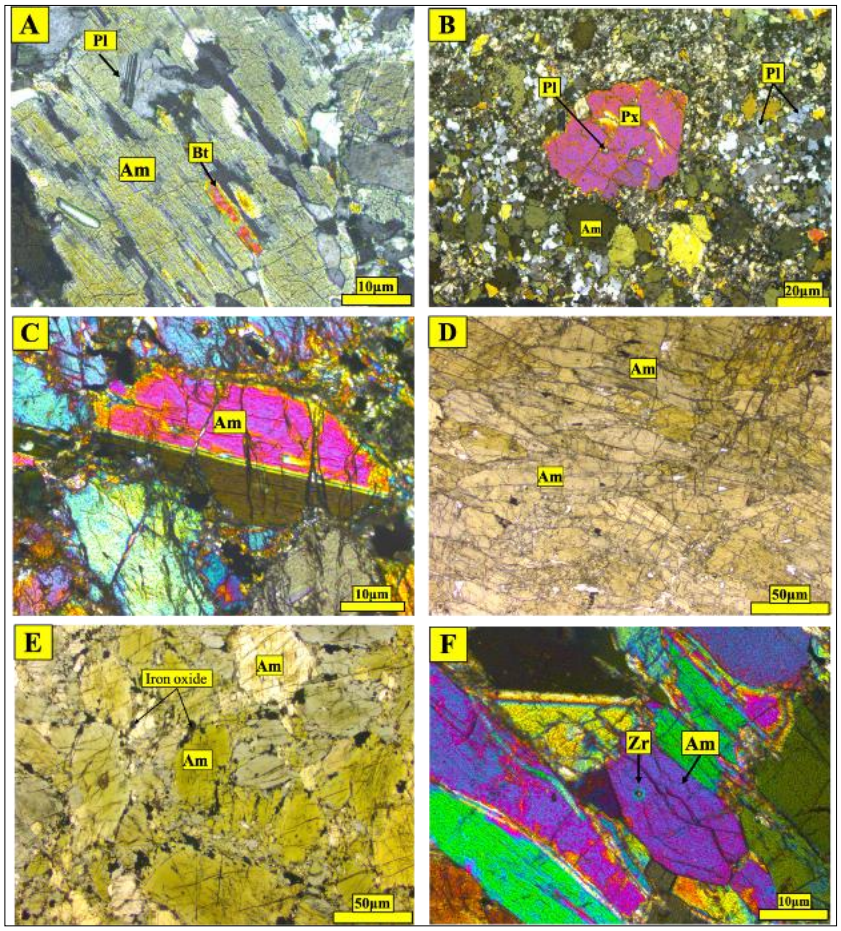


Fig. 4. Photomicrographs of amphibolite and hornblendite rocks: (A) Plagioclase and biotite as inclusions within amphibole in amphibolite (XPL); (B) blasto-subophitic and blasto-ophitic texture, showing relic clinopyroxene partly and completely enclosing plagioclase inclusion in amphibolite (XPL); (C) Amphibole grain illustrating Carlsbad twinning in hornblendite (XPL); (D) Amphibole grains aligned parallel to the rock foliation in hornblendite (PPL); (E) opaque grains occur as interstitial grains between amphibole grains and some of them are oriented along grain boundaries of coarse-grained hornblende in hornblendite (PPL); (F) Tiny inclusion of zircon enclosed by amphibole crystal, characterized by pleochroic halos due to radiation in hornblendite (XPL).

Opaque grains range in shape from euhedral to anhedral, typically occur as oriented grains along crystal boundaries (Fig. 3F), and also occur as polygonal, and irregular inclusions within amphibole. Some hornblende grains contain numerous, oriented, and tiny opaque inclusions. EPMA-BSE images reveal that ilmenite occurs as fine crystals along amphibole boundaries and as inclusions in sphene and amphibole (Fig. 5D). Magnetite inclusions exist in amphibole and in altered plagioclase (Fig. 5C) or larger crystals/clusters associated with ilmenite. Ilmenite grains are mostly associated with titanite, and can be seen as inclusions in sphene (Fig. 5D). Inclusions of zircon and apatite occur in amphibole (Fig. 5D).

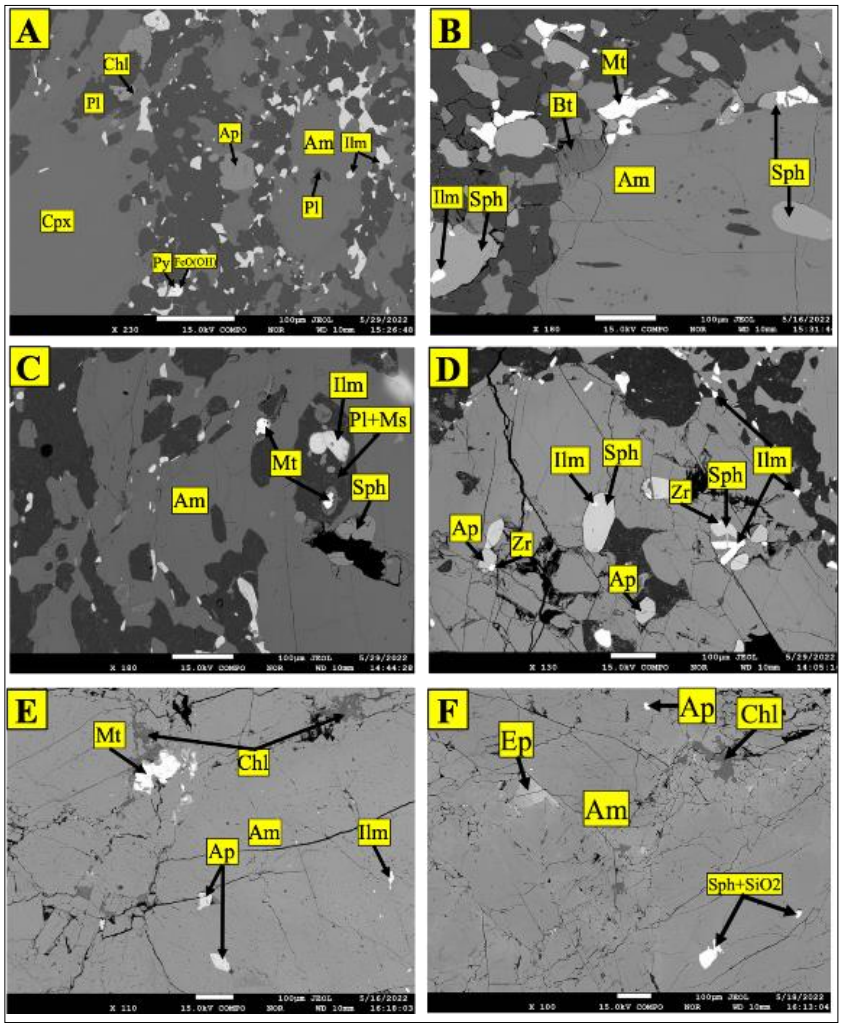


Fig. 5. EPMA-BSE images illustrating the petrographic characteristics of the studied samples from Bulfat area: (A) magnetite grains along amphibole boundaries and fine grains of plagioclase, ilmenite, and apatite within the banded amphibolite matrix *;* (B) Core of sphene contain inclusion of ilmenite, fine grains of biotite in groundmass next to amphibole, and sphene and plagioclase as inclusion in amphibole in banded amphibolite*;* (C) Amphibole phenocryst contains plagioclase which is partially altered to muscovite (sericite), and contains magnetite and ilmenite inclusions in massive amphibolite*;* (D) Amphibole grain contains apatite, ilmenite, zircon, and sphene inclusions; ilmenite grains occur along the amphibole boundaries and as inclusion in sphene within massive amphibolite*;* (E) Amphibole crystal contains tiny inclusions of apatite, chlorite, ilmenite, and magnetite in hornblendite*;* (F) Chlorite, apatite, epidote, and spinel + SiO_2 inclusions within hornblende grains in hornblendite.

4.1.3. Hornblendite

Primary minerals in hornblendite rocks include amphibole (>90) which is the most abundant mineral, followed by ± pyroxene (5%), + opaque (<4%), ± plagioclase (<1%), ±titanite (<1%), ±quartz (<1%), ± calcite (<1%), ± apatite (<1%), ± zircon (<1%), ± biotite (<1%), and ± chlorite (<1%). The main textures encountered within hornblendite rocks are foliation (Fig. 4D), equigranular (Fig. 4E), and poikilitic (Fig. 4F).

Amphibole crystals are euhedral to anhedral, equigranular, coarse- (5mm) to fine-grained (<1 mm) and contain quartz, apatite, rutile, and zircon inclusions. It is mostly green in colour, has strong pleochroism, symmetrical extinction and is commonly twinned (Fig. 4C). In some sample, hornblende grains are aligned along lineation direction (Fig. 4D). Sometimes, euhedral crystals of hornblende are

enclosed in secondary amphibole. Some crystals show zoning or undulose extinction. Altered hornblendes show chlorite along the boundaries and fracture as a result of their chloritization (Figs. 5E, F).

Actinolite is characterized by yellow to pale bluish green pleochroism, medium relief, and high interference colors (Fig. 4E). Their extinction angle ranges between 0° to 20° parallel to the lineation of columnar crystal. Basal sections show rhombic crystals with symmetrical extinction, and two sets of cleavage at angles of 56° and 124° (Fig. 4F). Actinolite is the product of alteration of hornblende during retrograde metamorphism. Many actinolite crystals show twining (Fig. 4F). Pyroxene is rare and anhedral, and spread as small crystals around coarse-crystals of hornblende. Zircon occurs as an inclusion in amphibole crystals which are surrounded by pleochroic halos (Fig. 4F).

Opaque grains are euhedral to anhedral, typically oriented along hornblende boundaries, or as interstitial grains between amphibole grains (Fig. 4E). Opaque grains appear as small (<5 μm), rounded, polygon, or irregular inclusions within amphibole or as fine grains in groundmass (Fig. 4E). Based on EPMA-BSE image, ilmenite grains occur among amphibole crystals or as inclusions in amphibole (Fig. 5E), or replaced by sphene and rutile. Magnetite is rare and occurs along amphibole crystal boundaries (Fig. 5E). Cr-spinel (chromite) exists in amphibole as inclusion and is usually altered (altered parts/rims marked as Spinel and quartz. in the BSE images, spinel presents as Fe+Cr+Mg+Al and Si type, and it occurs between amphibole grains or as inclusions within amphiboles (Fig. 5F). Apatite is euhedral to anhedral, high relief, shows low interference colour, and occur as tiny inclusion in amphibole (Figs. 5E & 5F). Chlorite is restricted to the cracks, fractures, and grain boundaries and as inclusion (Figs. 5E & 5F).

4.2. Mineral Chemistry

Major and minor element compositions of amphibole, plagioclase, pyroxene, and Fe-Ti oxides were analyzed on polished thin sections by EPMA. In total six samples have been chosen from banded amphibolite, massive amphibolite and hornblendite, (two samples from each group) and analysed to determine the chemical composition and to classify the rock samples.

4.2.1. Amphibole

Amphiboles of the banded amphibolite show variation in their silica (si) content ranging from 6.12-7.83 atom per formula unit (apfu), the Na of the B-site (Na_B) is <0.67, the Mg#:Mg/(Mg + Fe^{2+}) ranges between 0.58 to 0.98, and the Ca content of B-site (Ca_B) ranges between 1.69 to 2 apfu . The samples are nearly equally divided between tshermakite, magnesio-hornblende and pargasite fields according to the occupancy of B sites $(Ca+Na)_B$ in the Si in formula versus Mg#:Mg/($Mg+Fe^{2+}$) diagram of Leake et al (1997) (Table 1; Figs. 6A, B).

Table 1. amphibole composition and its formula in studied samples calculated to 23 Oxygen

Rock type	Banded amphibolite				Massive amphibolite					Hornblendite				
Sample no.	**GJ3**	**GJ3**	**BJ4**	**BJ4**	**AHJ4**	**AHJ4**	**AHJ4**	**GJ10**	**GJ10**	**SHJ3**	**SHJ3**	**HAJ1**	**HAJ1**	**HAJ1**
Analyses spot	**4**	**5**	**369**	**380**	**89**	**99**	**107**	**312**	**362**	**64**	**86**	**251**	**290**	**301**
SiO_2	41.27	53.8	41.74	55.11	54.68	44.05	43.84	44.96	42.89	42.67	50.15	43.05	41.57	46.02
TiO_2	2.06	0.39	0.93	0.07	0.09	0.34	0	1.36	1.68	1.04	0.43	0.68	0.76	0.54
Al_2O_3	11.11	2.51	11.34	1.34	2.07	12.75	37.26	8.61	10.83	14.71	8.36	14.09	15.37	11.84
FeO	16.88	10.82	13.79	8.59	9.89	13.82	0.26	15.12	15.52	8.60	5.97	10.91	10.86	9.15
MnO	0.28	0.22	0.23	0.21	0.22	0.20	0.01	0.35	0.30	0.11	0.10	0.19	0.17	0.20
MgO	10.22	16.61	12.04	18.32	16.92	11.14	0.01	11.70	10.7	15.20	18.58	13.75	13.19	15.90
CaO	11.00	12.05	11.62	12.36	12.54	12.26	19.32	11.61	11.62	11.54	11.61	11.48	11.36	11.13
Na_2O	2.36	0.64	1.75	0.23	0.09	1.24	0.27	1.36	1.62	2.36	1.51	2.42	2.48	1.96
K_2O	0.80	0.09	0.35	0.03	0.02	0.03	0.00	0.49	0.66	0.28	0.04	0.14	0.17	0.14
Cr_2O_3	0.02	0.00	0.06	0.02	0.04	0.01	0.00	0.01	0.08	0.09	0.11	0.17	0.04	0.10
Total	96.00	97.12	93.85	96.27	96.57	95.84	100.97	95.57	95.91	96.60	96.89	96.85	95.97	96.98
T: Si	6.27	7.68	6.35	7.84	7.82	6.53	6.48	6.76	6.47	6.11	6.99	6.21	6.06	6.50
Al^{iv}	1.73	0.32	1.66	0.16	0.18	1.47	1.52	1.25	1.53	1.89	1.01	1.79	1.94	1.49
Fe^{3+}	0.00	0.00	0.00	0.00	0.00	0.00	0.00	0.00	0.00	0.00	0.00	0.00	0.00	0.00
Ti	0.00	0.00	0.00	0.00	0.00	0.00	0.00	0.00	0.00	0.00	0.00	0.00	0.00	0.00
C: Al^{vi}	0.26	0.11	0.38	0.06	0.17	0.76	4.96	0.28	0.39	0.59	0.37	0.61	0.70	0.48
Ti	0.24	0.04	0.11	0.01	0.01	0.04	0.00	0.15	0.19	0.11	0.05	0.07	0.08	0.06
Fe^{3+}	0.55	0.25	0.69	0.25	0.11	0.38	0.00	0.43	0.39	0.82	0.65	0.76	0.79	0.96
Cr	0.00	0.00	0.01	0.00	0.00	0.00	0.00	0.00	0.01	0.01	0.01	0.02	0.00	0.01
Mg	2.32	3.54	2.73	3.88	3.61	2.46	0.00	2.62	2.41	3.24	3.86	2.96	2.87	3.35
Fe^{2+}	1.59	1.04	1.06	0.77	1.07	1.34	0.03	1.47	1.57	0.21	0.05	0.56	0.54	0.12
Mn	0.04	0.03	0.03	0.03	0.03	0.03	0.00	0.04	0.04	0.01	0.01	0.02	0.02	0.02
Ca	0.00	0.00	0.00	0.00	0.00	0.00	0.00	0.00	0.00	0.00	0.00	0.00	0.00	0.00
B: Ca	1.79	1.84	1.89	1.88	1.92	1.95	2.0	1.87	1.88	1.77	1.73	1.78	1.78	1.69
Na	0.21	0.16	0.11	0.06	0.03	0.05	0.00	0.13	0.12	0.23	0.27	0.23	0.23	0.32
A: Ca	0.00	0.00	0.00	0.00	0.00	0.00	1.06	0.00	0.00	0.00	0.00	0.00	0.00	0.00
Na	0.49	0.02	0.41	0.00	0.00	0.30	0.08	0.27	0.35	0.43	0.14	0.45	0.48	0.22
K	0.16	0.02	0.07	0.01	0.00	0.01	0.00	0.09	0.13	0.05	0.01	0.03	0.03	0.03
$M/(M+Fe^{2+})$	0.59	0.77	0.72	0.84	0.77	0.648	0.07	0.64	0.61	0.94	0.99	0.84	0.84	0.96

In massive amphibolites, the composition of the amphiboles is mostly magnesio-hornblende and fewer actinolites; their Si in formula varies between 6.397 to 7.875 apfu, and Mg# ranging between 0.07 to 0.966 (Fig. 6A). Both types of amphiboles in massive amphibolite are characterized by low Ti ranging between 0.005-0.017 apfu and low Al^{IV} ranging varies 0.0903 to 0.426 apfu. Amphiboles of hornblendites are predominantly tschermakite with minor magnesio-hornblende and pargasite; their Mg# = 0.87–0.97, Si = 6.10–6.78 pfu, Al^{IV} = 1.235–2.027 apfu, $(Na + K)_A$ = 0.027–0.241 apfu, and TiO_2 = 0.368–1.024 wt% based on the nomenclature of Leake et al. (1997) (Figs. 6A, 6).

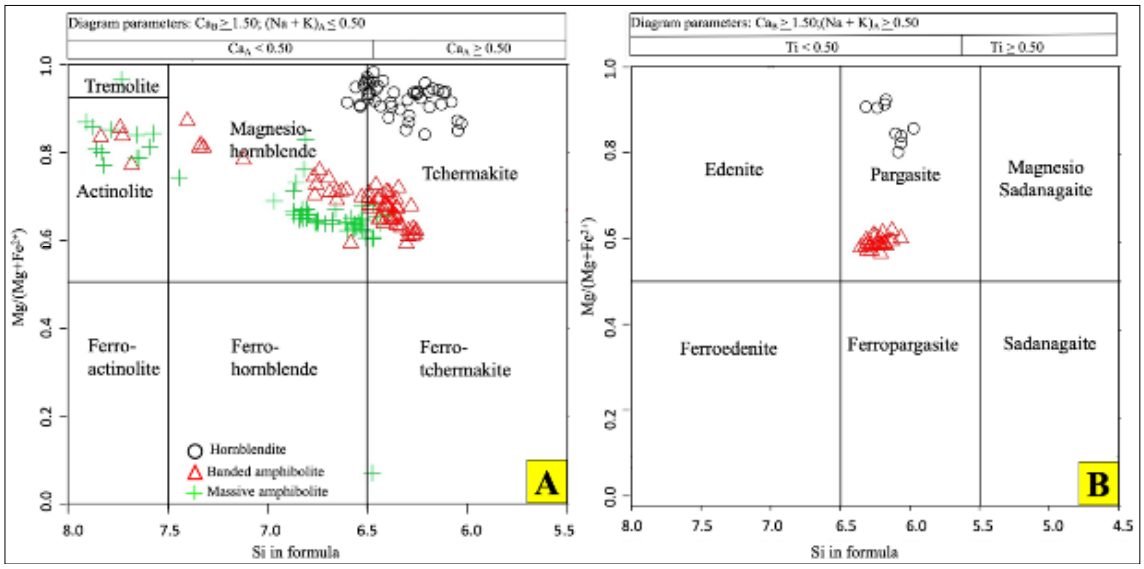


Fig. 6. Chemical classification diagram of the calcic amphiboles for the studied samples (Leake et al., 1997).

4.2.2. Plagioclase

Plagioclases in banded amphibolite samples are plotted on the ternary Ab-An-Or classification diagram (Deer et al., 1963) showing Na-rich composition, which are mainly oligoclase and andesine, with less albite component whose average end-member formula is $An_{14.911}\,Ab_{84.826}\,Or_{0.262}$" in GJ3 and is "$An_{32.269}\,Ab_{67.4878}\,Or_{0.243}$" in BJ4 (Fig. 7A and Table 2).

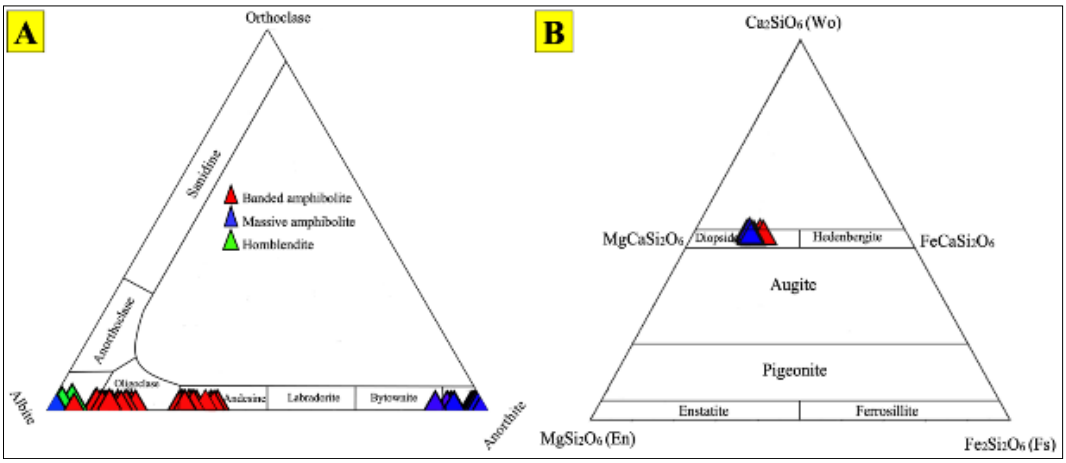


Fig. 7. (A) Feldspar classification diagram (Ab-An-Or) (Deer et al., 1963); (B) Clinopyroxene classification diagram (En-Wo-Fs) (Morimoto et al., 1988).

However, plagioclases of massive amphibolite have significantly higher anorthite (An) contents ($An_{88.06–99.06}$), which are mostly anorthite and few bytownite with average "$An_{0.916}\,Ab_{98.30}Or_{0.774}$"; very few samples have albite composition with average end-member formula "$An_{0.916}\,Ab_{98.30}Or_{0.774}$" (Fig. 7A). In hornblendites, plagioclase is rare and have albite composition ($An_{2.916}\,Ab_{97.014}Or_{0.069}$).

Table 2. Electron microprobe analyses of feldspar in the studied rocks; their formula is calculated according to 32 Oxygen.

Rock type	**Banded amphibolite**				**Massive amphibolite**				**Hornblendite**	
S. No. Analyses spot	**GJ312**	**GJ337**	**BJ4384**	**BJ4406**	**AHJ498**	**AHJ4138**	**GJ10317**	**GJ10343**	**HAJ1273**	**HAJ1275**
SiO_2	65.13	63.56	60.62	66.52	44.66	45.95	67.632	67.649	68.32	67.35
TiO_2	0.04	0.01	0.01	0.01	0.04	0.01	0	0.008	0.00	0.01
Al_2O_3	22.55	23.89	25.44	21.16	30.25	35.48	20.067	20.396	20.55	21.08
FeO	0.12	0.07	0.17	0.40	3.05	0.17	0.095	0.131	0.09	0.16
MnO	0.00	0.01	0.01	0.02	0.02	0.02	0.009	0.017	0.00	0.03
MgO	0.00	0.00	0.01	0.00	3.23	0.00	0	0	0.00	0.00
CaO	2.75	4.09	6.09	1.24	17.3	17.54	0.202	0.18	0.53	1.15
Na_2O	9.88	9.04	7.69	10.73	0.37	1.31	11.105	11.053	10.76	10.67
K_2O	0.01	0.06	0.02	0.04	0.01	0.01	0.026	0.195	0.02	0.02
BaO	0.01	0.03	0.00	0.01	0.00	0.00	0.000	0.000	0.00	0.00
Total	100.46	100.75	100.06	100.12	98.96	100.48	99.136	99.626	100.26	100.46
Si	11.40	11.14	10.75	11.66	8.45	8.41	11.903	11.860	11.88	11.73
Ti	0.01	0.00	0.00	0.00	0.01	0.00	0.000	0.001	0.00	0.00
Al	4.65	4.93	5.32	4.37	6.74	7.65	4.162	4.214	4.21	4.33
Fe(ii)	0.02	0.01	0.03	0.06	0.48	0.03	0.014	0.019	0.01	0.02
Mn	0.00	0.00	0.00	0.00	0.00	0.00	0.001	0.003	0.00	0.00
Mg	0.00	0.00	0.00	0.00	0.91	0.00	0.000	0.000	0.00	0.00
Ca	0.52	0.77	1.16	0.23	3.51	3.44	0.038	0.034	0.10	0.21
Na	3.35	3.07	2.65	3.65	0.14	0.46	3.789	3.757	3.63	3.60
K	0.00	0.01	0.01	0.01	0.00	0.00	0.006	0.044	0.00	0.01
Ba	0.00	0.00	0.00	0.00	0.00	0.00	0.000	0.000	0.00	0.00
An	13.32	19.94	30.38	5.99	96.23	88.07	0.994	0.882	2.62	5.61
Ab	86.63	79.80	69.49	93.80	3.73	11.86	98.854	97.981	97.28	94.27
Or	0.06	0.26	0.14	0.21	0.05	0.07	0.152	1.137	0.10	0.12

4.2.3. Pyroxene

According to EPMA analysis, pyroxene was observed in two samples (GJ10 and GJ3). The compositions of pyroxenes are plotted on the wollastonite-enstatite- ferrosilite ternary diagram of Morimoto et al (1988). All the analyzed pyroxenes from banded and massive amphibolite are Mg-rich and classified as diopside with end-member formula (Wo_{48} En_{37} Fs_{14}) in term of Fe-Mg ratio (Figs.7B).

4.2.4. Ilmenite

In banded amphibolites, ilmenites contain 42.46 - 47.2 wt% FeO, and 47.14 - 51.5 wt% TiO_2; meanwhile the ilmenites of the massive amphibolite contain 39.643 wt% FeO, and 50.58 wt% TiO_2. The ilmenites of hornblendite samples contain 42.46 - 47.2 wt% FeO and 49.18-51.17 wt% TiO_2.

4.3. Whole-rock geochemistry

The studied samples of banded amphibolite contain 0.69–1.98 wt% LOI, and are characterized by relatively higher SiO_2 contents of 49.8–50.51 wt% relative to the other rock types (Table 3). They also contain 7.04–8.86 wt% MgO, and 12.95 to 16.65 wt% Al_2O_3. These rocks have relatively high contents of $F_2O_{3(total)}$ (9.76–15.95 wt%), CaO (9.22–13.1 wt%), and TiO_2 (1.36–5.21 wt%), and low contents in MnO (0.15− 0.36 wt%) and P_2O_5 (0.07− 0.20 wt%). They also have high content of Cr, Sr, and low Rb, Sc. The light rare earth elements (LREEs) are slightly enrichment relative to the heavy rare earth elements (HREEs).

Table 3. Representative whole-rock geochemistry of amphibolite rocks in Bulfat area

Rock type	**Hornblendite**										
Samples no.	**LDL**	**ShJ2**	**ShJ3**	**ShJ8**	**ShJ5**	**HAJ1**	**HAJ3**	**HAJ5**	**HAJ8**	**HAJ9**	**GJ15**
Major and minor oxides (wt%)											
SiO_2	0.01	43.7	41.1	37.9	39.8	43.3	39.3	40	38.6	38.9	38.5
TiO_2	0.01	1.12	1.16	1.54	1.59	0.59	1.6	1.6	1.35	1.22	1.66
Al_2O_3	0.01	11.6	14.15	13.3	15.5	13.3	15.3	15.45	15.65	18.15	11.5
Fe_2O_3	0.01	9.84	10	13.6	11.4	11.4	13.4	13.75	14.45	12.95	11.5
MnO	0.01	0.13	0.12	0.14	0.13	0.17	0.16	0.16	0.14	0.11	0.13
MgO	0.01	16.3	15.5	12.65	14.55	15.2	12.6	12.65	13.85	12.35	12.3
CaO	0.01	12.15	12	13.1	12.45	11.25	11.5	11.5	11.4	12.2	16.5
Na_2O	0.01	2.02	2.44	2.03	2.61	2.25	2.71	2.71	2.24	2.27	1.54
K_2O	0.01	0.19	0.18	0.23	0.26	0.13	0.24	0.22	0.19	0.17	1
P_2O_5	0.01	0.29	0.18	1.96	0.56	0.02	0.03	0.03	0.2	0.13	1.31
Cr_2O_3	0.002	0.116	0.041	0.021	0.062	0.154	0.018	0.02	0.027	0.028	0.093
SrO	0.01	0.01	0.009	0.01	0.009	0.009	0.01	0.01	0.01	0.07	0.02
BaO	0.01	0.009	0.009	0.01	0.009	0.009	0.009	0.01	0.009	0.01	0.01
LOI	0.01	1.37	1.39	1.63	1.22	1.23	1.65	1.01	1.21	1.22	3.91
Total	100.29	98.84	98.26	98.13	100.14	98.99	98.52	99.12	99.32	99.78	99.97
Trace elements (ppm)											
Rb	0.2	0.3	0.3	0.4	0.5	0.3	0.7	0.9	0.4	0.3	4.5
Sr	0.1	158	112	227	218	56.4	147	141	169	727	253
Ba	0.5	19.7	13.3	46.8	26.7	10.6	32.8	50.3	25.8	60.4	113.5
Ni	1	238	239	109	166	421	145	150	123	163	187
Cr	10	890	290	150	450	1130	110	120	180	180	730
Ga	0.1	14	16.1	19.5	17.7	14.5	16.5	16.1	18	16.4	18.3
Nb	0.1	2.7	1.5	3	2.4	1.6	3.4	3	1.5	1.6	14.9
V	5	334	406	508	378	212	323	350	525	392	354
Y	0.1	15.7	22.3	31.2	25.3	14	36.8	35.7	26.9	24.4	27.8
Zn	2	52	38	63	56	60	70	77	38	31	145
Zr	2	99	45	148	96	32	50	51	58	66	404
Cs	0.01	0.02	0.02	0.02	0.04	0.01	0.02	0.04	0.02	0.03	0.14
Sc	1	63	63	63	63	28	36	35	56	46	30
Hf	0.1	3.8	1.8	5.5	3.5	1.2	2	2	2.1	2.3	9.5
Ta	0.1	0.1	0.09	0.09	0.09	0.09	0.09	0.09	0.09	0.09	0.2

Th	0.05	0.86	0.18	1.02	0.26	0.09	0.08	0.06	0.13	0.27	1.32
U	0.05	0.52	0.21	1.19	0.21	0.05	0.11	0.09	0.3	0.3	1.02
Co	1	59	50	61	55	54	57	56	60	54	40
Cu	1	8	4	370	18	6	27	5	6	15	63
Pb	2	1.9	1.9	1.9	1.9	2	1.9	1.9	1.9	1.9	1.9
Ti	10	9.9	9.9	9.9	9.9	9.9	9.9	9.9	9.9	9.9	4.5
REE (ppm)											
La	0.1	11.8	5	38.5	10	2.4	2.9	2.9	3.9	4.2	26.6
Ce	0.1	44.4	19.3	115.5	36.2	9.8	12.2	12.4	13.4	13	84.2
Pr	0.02	8.04	3.69	18.85	6.48	1.62	2.64	2.64	2.62	2.5	14.7
Nd	0.1	39.5	21	91.7	34.7	8.3	16.6	17.2	14.8	14.1	72
Sm	0.03	9.24	5.87	19.7	8.89	2.56	6.11	6.15	5.03	4.66	15.45
Eu	0.02	2.3	1.69	4.36	2.14	0.92	1.65	1.75	1.36	1.3	3.25
Gd	0.05	7.5	5.86	13.65	7.56	2.72	7.46	6.98	5.56	5.12	11.05
Tb	0.01	0.77	0.78	1.4	0.92	0.82	0.4	1.12	0.83	0.77	1.1
Dy	0.05	3.9	4.55	6.75	5.38	4.98	2.6	7.1	5.14	4.99	7.61
Ho	0.01	0.64	0.85	1.14	0.89	0.98	0.54	1.32	0.97	0.91	1.51
Er	0.03	1.58	2.33	2.81	2.68	2.91	1.63	4.09	3.07	2.76	4.56
Tm	0.01	0.17	0.3	0.31	0.31	0.4	0.21	0.55	0.39	0.37	0.65
Yb	0.03	1.14	1.76	2.02	2.13	2.67	1.5	3.17	2.34	2.27	3.87
Lu	0.01	0.17	0.25	0.29	0.29	0.39	0.21	0.47	0.39	0.36	0.63
∑REE	_	131.2	73.2	317.0	118.6	75.9	35.41	67.38	59.8	57.3	87.0
(Gd/Yb)n	_	5.32	2.69	5.47	2.87	1.47	1.90	1.759	1.92	1.82	4.61
(La/Sm)n	_	0.80	0.53	1.22	0.70	0.59	0.30	0.294	0.48	0.56	1.08
(La/Yb)n	_	7.03	1.93	12.95	3.19	1.09	0.62	0.61	1.13	1.26	9.31
Eu/Eu*	_	0.84	0.88	0.81	0.80	1.06	0.74	0.814	0.78	0.81	0.76

Table 3. (Continuation)

Rock type	**Banded amphibolite**							**Massive amphibolite**				
Samples no.	**BJ2**	**BJ3**	**BJ4**	**BJ5**	**GJ3**	**GJ8**	**GJ18**	**GJ10**	**AhJ1**	**AhJ2**	**AhJ4**	**AhJ5**
Major and minor oxides (wt%)												
SiO_2	48.5	49.8	46.7	49.5	44.2	48.5	48.8	48.5	40.8	40.9	48.2	37.4
TiO_2	1.36	1.55	1.7	1.74	5.21	1.8	1.47	2	2.32	2.24	0.28	0.98
$Al2O_3$	15.35	16.15	16.65	16.55	12.95	14.75	14.9	14.4	13.9	13.85	17.55	18.85
$Fe2O_3$	9.76	10.65	10.6	10.4	15.95	11.2	10.1	11.55	15.55	15.15	8.82	11.35
MnO	0.15	0.17	0.18	0.16	0.2	0.17	0.16	0.17	0.21	0.22	0.13	0.13
MgO	8.54	7.11	7.31	7.04	7.01	7.39	8.86	6.45	10.05	10.05	9.77	13.6
CaO	10.55	10.3	13.1	9.49	9.22	10	10.55	8.62	13.2	12.8	14.9	11.9
Na_2O	2.73	3.73	3.12	4.07	4.14	3.68	3.08	3.69	1.39	1.42	0.69	2.24
K_2O	1.2	0.43	0.81	0.25	0.31	0.71	0.19	0.96	0.41	0.52	0.01	0.16
P_2O_5	0.09	0.16	0.2	0.2	0.09	0.2	0.23	0.21	0.23	0.24	0.009	0.46
Cr_2O_3	0.049	0.049	0.056	0.039	0.004	0.051	0.059	0.04	0.039	0.051	0.021	0.033
SrO	0.02	0.02	0.01	0.03	0.01	0.02	0.02	0.03	0.009	0.009	0.009	0.02
BaO	0.01	0.01	0.01	0.01	0.01	0.02	0.01	0.01	0.01	0.01	0.009	0.009
LOI	1.98	1.12	0.75	0.7	0.94	1.42	0.69	1.64	2.17	2.01	1.43	2.88
Total	100.29	101.25	101.20	100.18	100.24	99.91	99.12	98.27	100.28	99.46	101.80	100.00
Trace elements (ppm)												
Rb	20.5	6.2	5.4	2	2.5	8.2	1.2	13.2	7.8	11	0.1	0.5
Sr	258	273	185.5	284	174	260	226	339	76.8	4	83.5	304
Ba	108.5	88.2	66.1	112	41.9	132.5	43.4	86.3	87.4	85.5	6.2	13.8

Ni	124	81	171	126	74	116	185	99	116	136	76	142
Cr	350	340	380	270	10	350	400	270	270	350	130	220
Ga	15.9	16.2	16.2	16.5	17.7	16.7	15.1	17.5	18.4	18	11.7	15.2
Nb	1.7	4.8	9.6	6.7	4.1	6.3	12.6	7.4	4.8	4.4	0.09	1.6
V	261	242	268	242	920	279	213	310	431	395	569	289
Y	25.2	30.7	31.1	30	28.7	35.7	23.9	38.8	46.8	45.9	2.2	27.1
Zn	54	62	96	65	79	80	86	75	95	93	33	40
Zr	67	128	128	131	110	125	127	143	108	106	1.9	84
Cs	0.05	0.05	0.06	0.03	0.4	0.04	0.05	0.19	0.05	0.06	0.03	0.11
Sc	63	63	63	63	63	63	30	35	54	53	58	37
Hf	1.7	3.2	3.2	3.2	2.7	3.2	3	3.6	3.1	3.1	0.09	2.7
Ta	0.09	0.3	0.5	0.4	0.3	0.3	0.7	0.5	0.2	0.1	0.09	0.09
Th	0.18	0.53	0.69	0.38	0.2	0.57	0.54	0.94	0.54	0.68	0.04	0.27
U	0.09	0.15	0.16	0.23	0.2	0.2	0.16	0.25	0.23	0.19	0.04	0.86
Co	46	38	45	42	47	40	0.9	40	46	60	62	49
Cu	40	55	21	80	54	59	52	63	87	163	148	78
Pb	1.9	1.9	1.9	3	1.9	1.9	47	1.9	1.9	1.9	1.9	1.9
Ti	9.9	9.9	9.9	9.9	9.9	10	1.9	9.9	9.9	9.9	9.9	9.9
REE (ppm)												
La	2.6	5.6	6.8	5	2.7	6.7	9.5	8.4	7.9	7.4	0.09	6.5
Ce	8.1	15.6	17.7	14.2	8.3	19	25.5	23.3	22.8	20.7	0.1	20.2
Pr	1.48	2.41	2.73	2.23	1.48	2.97	3.59	3.53	3.63	3.43	0.03	3.56
Nd	8.6	12.9	13.8	11.5	8.4	14.6	16.3	17.8	19	17.3	0.2	19.4
Sm	3.1	4.02	4.26	3.71	3.11	4.57	4.31	5.4	5.74	5.86	0.1	5.88
Eu	1.11	1.28	1.36	1.14	1.14	1.3	1.26	1.69	1.85	1.75	0.09	1.64
Gd	3.89	4.97	5.68	4.63	4.33	5.71	4.56	6.97	7.84	7.5	0.21	5.55
Tb	0.68	0.82	0.85	0.78	0.7	0.92	1.24	1.1	0.75	1.22	1.22	0.04
Dy	4.6	5.8	6.12	5.45	5.26	6.32	6.17	7.61	4.42	8.17	8.44	0.4
Ho	0.9	1.16	1.17	1.12	1.01	1.29	1.01	1.51	0.92	1.65	1.66	0.08
Er	2.73	3.51	3.71	3.14	3.23	3.92	2.58	4.56	2.79	5.08	4.93	0.3
Tm	0.4	0.46	0.51	0.43	0.45	0.54	0.3	0.65	0.36	0.68	0.67	0.03
Yb	2.49	3.05	3.04	2.91	2.88	3.41	1.94	3.87	2.35	4.21	4.38	0.31
Lu	0.35	0.47	0.48	0.44	0.45	0.57	0.27	0.63	0.35	0.64	0.63	0.04
∑REE	41.0	62.1	68.2	56.7	43.4	71.8	240.8	87.0	77.0	90.4	85.9	1.9
(Gd/Yb)n	1.26	1.32	1.51	1.29	1.22	1.35	1.57	1.46	1.51	1.39	0.55	1.68
(La/Sm)n	0.52	0.87	1.00	0.84	0.54	0.92	1.38	0.97	0.86	0.79	0.56	0.58
(La/Yb)n	0.71	1.25	152.00	1.17	0.64	1.33	2.75	1.47	1.27	1.15	0.2	1.65
Eu/Eu*	0.97	0.87	0.84	0.84	0.95	0.78	0.87	0.84	0.84	0.80	1.89	0.88

By contrast, the massive amphibolites are characterized by low SiO_2 (37.4.5 - 40.9 wt%), high Al_2O_3 (13.9-18.85 wt%) and MgO (6.45 - 13.6 wt%); the $Fe_2O_{3(total)}$ of massive amphibolites various between 8.82 to 15.55 wt%, and have lower TiO_2 (0.28-2.32%) content. Most REE in massive amphibolite samples have relatively consistent content except one sample which has low $HRREE_S$ and $LREE_S$. Samples of this rock show mostly high Sr, Ba, Cr, Ni, and low Ta, Th, and U content.

The hornblendites are characterized amphibolites by having relatively lower concentrations of SiO_2, MnO, Na_2O, K_2O, TiO_2, Rb, Ba, Cs, Zr and HREEs, and higher concentrations of MgO, CaO, and Ni. The LREEs content in hornblendites are relatively higher than the banded amphibolites and lower than the massive amphibolites. They mostly have lower Sr content than the banded amphibolites, and higher than the massive amphibolites with the exception of one sample (HAJ9) which have very high concentration of Sr.

The primitive mantle-normalized trace elements spider diagram of Sun and McDonough (1989) shows that the banded amphibolites have positive Ba, K, Pb, Sr, Zr, and Ti anomalies, and negative Rb, Th, Nb, Pr, P, Eu, and Yb anomalies. In contrast, the massive amphibolites are characterized by negative Th, Nb, Sr, Zr, and Ti anomalies, and positive Rb, U, La, Sm, and Dy anomalies. The hornblendite relative to other both types of amphibolites is richer in Pr, Nd, P, U, La, Ce, Sm, Eu, and poorer in Cs, Rb, Nb, K, Ti, Y, and HREE, with distinct positive anomalies for Ba, U, Dy, and Sm and negative anomalies for Rb, Nb, Zr, Ti, and Sr (Fig. 8A). There is enrichment of LREE in hornblendites, such as La, Ce, Pr, and Nd. There are strong negative Ti anomalies and slight negative Zr anomalies in all samples.

On chondrite-normalized REE diagram of Boynton (1984), both banded and massive amphibolites show close values and similar patterns which are distinct from that of hornblendite (Fig. 8B). The amphibolites are enriched in LRRE due to partial melting and fractional crystallization (banded amphibolite with La/Sm = 0.52–1.38; La/Yb = 0.71–1.52 and massive amphibolite with "La/Sm = 0.79–0.97; La/Yb= 0.80–1.89" and depleted in HRRE "banded amphibolite with Gd/Yb = 1.22–1.57 and massive amphibolite with "Gd/Yb = 0.55–1.68" (Fig. 8B). However, the hornblendites are more enriched in LRRE (Pr, Nd, and Pm are more enriched than La and Ce) (La/Sm = 0.3–1.22; La/Yb = 0.62–12.95), and more depleted in HRRE patterns (Gd/Yb =1.47–5.32) relative to both amphibolites.

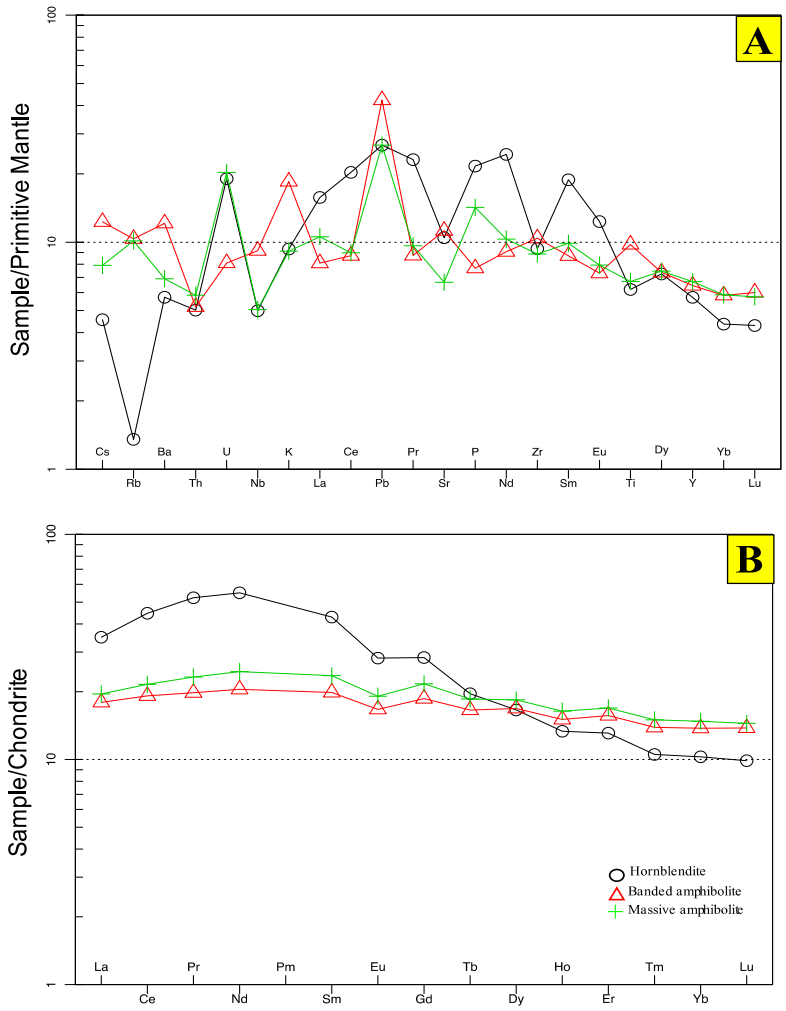


Fig. 8. (A) mantle-normalized trace element spider diagrams for amphibolite rocks (Sun and McDonough, 1989); (B) chondrite-normalized REE patterns (Boynton, 1984). It is plotted on semi-log. Circles are hornblendites, Crosses are massive amphibolites, and triangles are banded amphibolites.

4.4 Geothermobarometry

Amphiboles, particularly hornblende, are the most commonly utilized minerals for geothermobarometry because they can be found in a variety of calc-alkaline intrusive rocks (Sheikhi et al., 2020). Based on the mineral assemblages of amphibole and plagioclase from all banded amphibolite, massive amphibolite, and hornblendite, the temperature calculation was carried out using hornblende and hornblende-plagioclase geothermometers (Otten, 1984; Colombi, 1989; Blundy and Holland, 1990; Ernst and Liu, 1998).

Ti in amphibole thermometry of Colombi (1989) indicates temperatures of 547–884 ◦C for banded amphibolite, 445–796 ◦C for massive amphibolite and 556–728 ◦C for hornblendite. Meanwhile, Ti in amphibole thermometry of Otten (1984), shows temperatures of 553–894 ◦C for banded amphibolite, 545–796 ◦C for massive amphibolite and 593 ◦C–702 ◦C for hornblendite. Hornblende-plagioclase compositions were measured as a geothermometer by Blundy and Holland in 1990. The calculated results for banded amphibolite, massive amphibolite and hornblendite show temperature ranges of 719–848 oC, 663–684 oC, and 620–646 oC, except for one sample of massive amphibolite (AHJ4) with high Ca content (An88.06–99.06) gives very high temperature.

Ti and Al in amphibole are used as temperature and pressure indicators by Ernst and Liu (1998) based on the TiO_2- Al_2O_3 isopleth from amphibole composition. By using this geothermometer, the calculated temperature range is between 400 and 850 ˚C for banded amphibolite and 400–793 ˚C for massive amphibolite (Fig. 9). The majority of amphibolite lies between 3-5 kbar as average, while banded amphibolite gives higher pressure conditions due to the composition of Al_2O_3 in amphibole (Fig. 9).

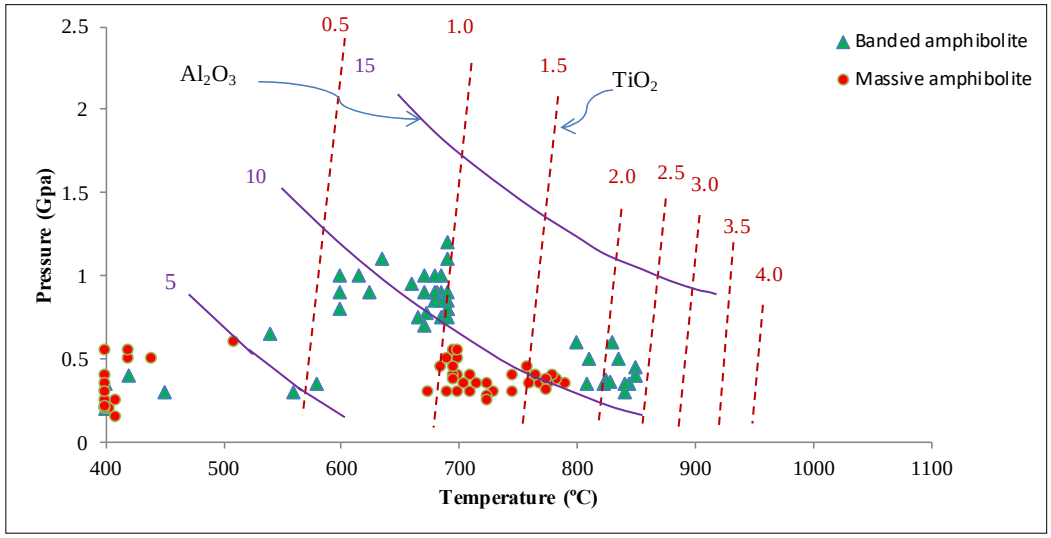


Fig. 9. Al_2O_3 and TiO_2 isopleths for amphibole in weight percent (Ernst and Liu, 1998) for amphibolite rocks.

5. Discussion

Based on the major element composition (Le Bas et al., 1986) (Fig. 10A), the banded amphibolites and massive amphibolites are classified as basalts with the exception of one sample which plots in the tephrite-basanite field; they are divided between alkaline and subalkaline/tholeiitic fields. The hornblendite rocks are divided between picrobasalts and foidites and the majority has alkaline affinity. On SiO_2 vs. FeO_t/MgO diagram (Miyashiro, 1974) the majority of amphibolites are tholeiites (Fig. 10B). According to MgO-FeO^T-Al_2O_3 diagram (Pearce et al., 1977) (Fig. 11A), both banded and massive amphibolite, and hornblendites fall in the field of oceanic ridge and floor. The La/Yb – Th/Nb diagram

of Hollocher et al (2012) (Fig. 11B) reveal that most of the banded and massive amphibolites plot in the field of mid-oceanic ridge basalt (MORB). The hornblendites show a wide scatter between MORB and other fields including alkaline arc, oceanic islands, and oceanic arcs. Based on triangular diagrams of Wood (1980) (Figs. 11C, D), the majority of banded and massive amphibolite fall in the field of N-MORB and fewer in E-MORB with few exceptions. Most hornblendite samples belonge to N-MORB with the exception of few samples which are scattered between the fields of island arc tholeiite basalt and E-MORB.

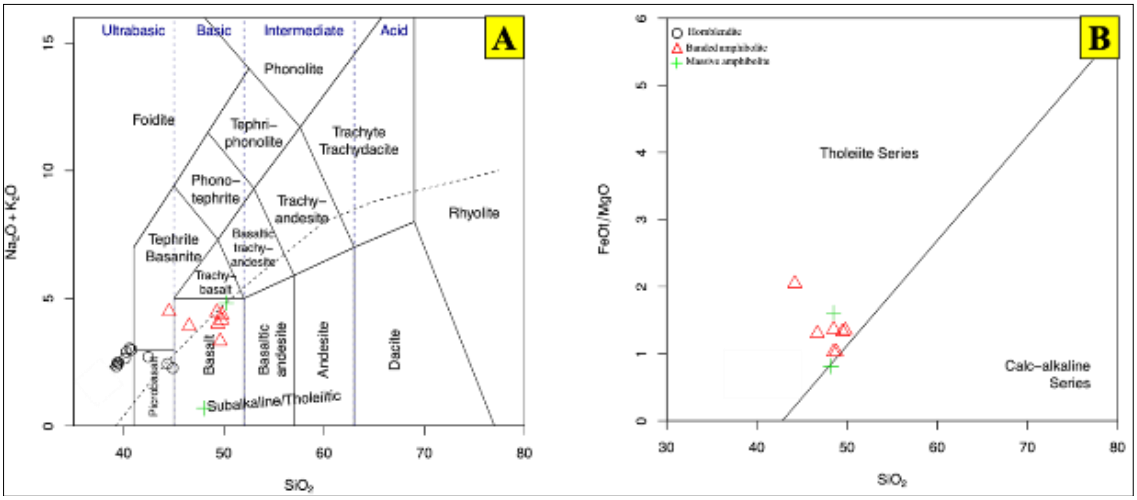


Fig. 10. (A) Chemical classification diagram of volcanic rocks (TAS) between SiO_2 versus Na_2O+K_2O (Le Bas et al.,1986); (B) FeO_t /MgO versus SiO_2 discrimination diagram (Miyashiro, 1974).

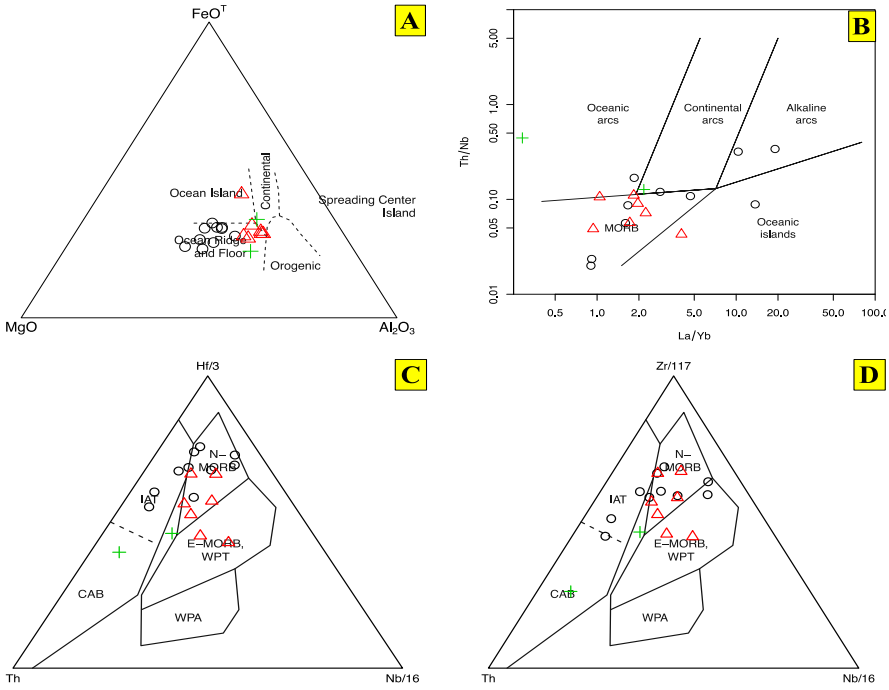


Fig. 11. Tectonic setting discrimination diagrams for the studied amphibolite rocks**:** (A) MgO-FeO^T-Al_2O_3 ternary discrimination diagram of Pearce et al. (1977); (B) The La/Yb – Th/Nb diagram of Hollocher et al (2012); (C)(D) Triangular diagrams of the Th-Hf-Zr-Nb system (wood, 1980). IAT; island arc tholeiite, CAB; calc-alkaline basalt, normal (N)-MORB, enriched (E)-MORB, WPA; within-plate alkaline, WPT; within-plate tholeiite.

The petrographic study results showed that the studied rocks were affected by different degrees of alteration, which resulted in the formation of secondary minerals such as sericite, chlorite, and epidote. Plagioclase grains in amphibolites show polysynthetic twinning, but some lack twinning because of the small size of grains. This agrees with what mentioned by Nesse (2000) stating that twining of plagioclase can be absent in small grains, especially in metamorphic rocks. The undulose extinction in some amphibole and plagioclase crystals is a deformation feature (Hadi et al., 2013). Pleochroic halos in hornblendite is due to radiation from radioactive trace elements in zircon inclusions.

One sample of hornblendite (HAJ9) has a higher concentration of Sr than other hornblendite samples because of the presence of a plagioclase vein in this sample. Hornblendite generally has a lower Sr content than banded amphibolites and a greater Sr content than massive amphibolites. One sample of hornblendite (HAJ9) has a higher concentration of Sr than other hornblendite samples because of the presence of a plagioclase vein in this sample. In all samples, there are significant negative Ti anomalies and minor negative Zr anomalies, which show the retention of refractory minerals such zircon-rutile, apatite, and sphene (Hadi., 2013). Both amphibolites and hornblendite typically show negative Eu anomalies indicating either that plagioclase fractionation occurs during magma development, or there was presence of plagioclase in the mantle source where partial melting occurred. The geochemical characteristics of most amphibolite samples indicate their igneous origin of tholeiitic basalt affinity with sub-alkaline basalt protoliths that are produced by fractionation of pyroxene and plagioclase.

During the closure of the Neotethyan Ocean several oceanic fragments (ophiolites) were obducted in the Zagros Suture Zone (Al Humadi et al., 2019). The Zagros Suture Zone is characterized by different tectonic units in several nappes and thrust sheets (Ali et al., 2014). Bulfat area is part of the ophiolite-bearing terranes (upper allochthon), which represents part of the second unit of the Penjween-Walash Subzone.

Geological history of the upper allochthon revealed that subduction was active during the Cretaceous period (Azizi and Jahangiri, 2008; Aswad et al., 2016). This was followed by, collision and obduction of the Cretaceous ophiolite complexes onto the northeastern margin of the Arabian Plate during the Late Cretaceous. However, The Bulfat Igneous Complex represents subduction zone of Eocene arc magmatism into the Cretaceous suprasubduction complex (Ali, 2017). Later rifting, led to ascending of the mantle upwelling and lithosphere to produce the melt that gave rise to the Wadi Rashid gabbro (Aswad et al., 2013) and olivine gabbro (Ali, 2017). N-MORB represents the main tectonic environment of most studied rocks, unlike previous studies that appeared E-MORB for rifting in Bulfat area (Aswad et al., 2013; Ali, 2017). Only two samples of banded amphibolite are plotted in the E-MORB field according to diagrams of wood (1980).

MORB geochemical signatures of the studied samples indicate that were they formed in an extensional tectonic environment, such as an intra-arc rift or a back arc. MORB are thought to be the products of comparatively large degree of partial melting; hence, their trace element patterns must reflect those of their mantle source. Therefore, the depletion of $LILE_s$ such as Rb, K, Sr, and Ba indicate to MORB character. Most banded amphibolite samples show the enrichment in $LILE_S$ such as Cs, Ba, K, Pb, and Sr which is related to alteration (unrelated to magma origin). In hornblendite, depletion in Rb and Cs belonged to N-MORB; while, there is enrichment in LREE relative to other trace elements and this suggests assimilation of country rock by magma, or because of the rift in back arc. Depletion in Nb is related to the NMORB environment, and most of the studied samples have $(La/Sm)_n$ <1, which is another indicator of the NMORB environment.

Typically, the metamorphic paragenesis that occurs in any metamorphic rocks is based on pressure and temperature reached during metamorphism, and the bulk composition of the protolith. Experimental petrography, in which the researcher determined the equilibrium temperature and pressure in the lab to the modal natural geological system, allows for the estimation of the metamorphic condition for paragenesis during metamorphism. (Winter, 2010).

All amphibolites in the Bulfat area have hornblende and plagioclase as major constituents and diopside. While sphene is a common accessory phase in banded amphibolite. According to the petrographic study, banded amphibolites have the following mineral assemblages: Hornblende + plagioclase ± clinopyroxene + sphene + iron oxides ± zircon ± apatite, ± biotite, ± apatite ± rutile ± zircon ± zeolite ± sericite ± chlorite ± epidote.

According to the petrographic study, massive amphibolites have the following mineral assemblages: Amphibole + plagioclase ± pyroxene ± apatite + opaque minerals + rutile.

By employing different geothermobarometers for the Bulfat amphibolite and according to the mineral assemblage of studied amphibolites. These conditions are corresponding to amphibolite facies.

6. Conclusions

The predominant mineral constituents in the banded and massive amphibolites are calcic amphiboles and plagioclase with minor to accessory minerals such as diopside, iron oxides, titanite, quartz, apatite, and zircon. The predominant minaral in hornblendites is amphibole with accessory minerals such as iron oxides, apatite, rutile, zircon, titanate, and chlorite.

The electron microprobe analysis (EPMA) showed that the amphiboles of the banded amphibolite are nearly equally divided between tschermakite, magnesio-hornblende and pargasite; and those of the massive amphibolites range between magnesio-hornblende and less actinolite; meanwhile those of hornblendites are dominantly tschermakite with minor magnesio-hornblende and pargasite. The plagioclase of banded amphibolites are mostly andesine and albite, and those of the massive amphibolites are mostly anorthite, meanwhile those of hornblendites are albite. P-T condition of metamorphism revealed that the studied amphibolite rocks are within amphibolite facies grade.

The main textures in amphibolite rocks are porphyroblastic, granoblastic, poikiloblastic, nematoblastic, and blasto-ophitic texture.

Chemical classification diagrams showed that most amphibolites have tholeiitic basaltic affinity, meanwhile the hornblendites are divided between picrobasalts and foidites.

Tectonic discriminating diagrams indicated MORB origin for most amphibolites, and MORB as well as Islan Arc Tholeiite origin for most hornblendites.

Primitive mantle-normalized trace element diagram, chondrite-normalized- REE patterns and tectonomagmatic discrimination diagrams reflected MORB origin for the studied rocks.

Acknowledgments: The authors are thankful to the Department of Applied Geoscience, University of Duhok for providing the opportunity for this study. We also thank the technical staff of the ALS Laboratory Group in Seville, Spain and the Institute of Petrology and Structural Geology, Charles University in Prague, Czech for their help in geochemical and mineralogical analyses. This paper is part of an ongoing M.Sc. thesis.

References

Abart, R., Schmud, R., Harlov, D., 2001. Metasomatic coronas around hornblendite xenoliths in granulite facies marble, Ivrea zone, N Italy, I: constraints on component mobility. Contributions to Mineralogy and Petrology, 141(4), 473-493.

Abdulnaby, W., 2019. Structural geology and neotectonics of Iraq, Northwest Zagros. In Developments in structural geology and tectonics, 3, 53.

Al Humadi, H., Väisänen, M., Ismail, S.A., Kara, J., O'Brien, H., Lahaye, Y., Lehtonen, M., 2019. U–Pb geochronology and Hf isotope data from the Late Cretaceous Mawat ophiolite, NE Iraq. Heliyon, 5(11), e02721.

Al-Qayim, B., Omer, A., Koyi, H., 2012. Tectonostratigraphic overview of the Zagros suture zone, Kurdistan region, Northeast Iraq. GeoArabia, 17(4),109-156.

Ali, S. A., Buckman S., Aswad K.J., Jones B.G., Ismail S.A., Nutman A. L., 2013. The tectonic evolution of a Neo-Tethyan (Eocene-Oligocene) island-arc (Walash and Naopurdan Groups) in the Kurdistan region of the northeast Iraqi Zagros Suture Zone. Island Arc, 22, 104-125.

Ali, S.A., Buckman, S., Aswad, K.J., Jones, B.G., Ismail, S.A., Nutman, A.P., 2012. Recognition of Late Cretaceous Hasanbag ophiolite-arc rocks in the Kurdistan region of the Iraqi Zagros Thrust Zone: A missing link in the paleogeography of the closing Neo-Tethys Ocean. Lithosphere., 4, 395-410.

Ali, S.A., 2017. 39 Ma U-Pb zircon age for the Shaki-Rash gabbro in the Bulfat igneous complex, Kurdistan region, Iraqi Zagros Suture zone: rifting of an Intra-Neotethys Cenozoic arc. Ofioliti, 42(2),69-80.

Aswad K.J., Aziz, N.R., Koyi, H.A., 2011. Cr-spinel compositions in serpentinites and their implications for the petrotectonic history of the Zagros Suture Zone, Kurdistan Region, Iraq. Geological Magazine, 148 (5-6), 802-818.

Aswad, K.J., Sheraefya, R.M., Ali, S.A., 2013. Pre-collisional intrusive magmatism in the Bulfat Complex, Wadi Rashid, Qala Diza, NE Iraq: Geochemical and mineralogical constraints and implications for tectonic evolution of granitoid-gabbro suites. Iraqi National Journal of Earth Sciences, 13, 103-137.

Aswad, K.J., Ali, S.A., Al-Sheraefy, R.M., Nutman, A.P., Jones, B.G., Buckman, S., Jourdand, F., 2016. $^{40}Ar/^{39}Ar$ hornblende and biotite geochronology of the Bulfat Igneous Complex, Zagros Suture Zone, NE Iraq: New insights on complexities of Paleo- gene arc magmatism during closure of the Neotethys Ocean. Lithos., 266-267, 406-413.

Azizi, H., Jahangiri, A., 2008. Cretaceous subduction-related volcanism in the northern Sanandaj-Sirjan Zone, Iran. J. Geodyn., 45, 178-190.

Bali, E., Hidas, K., Guðfinnsson, G.H., Kovács, Z., Török, K., Román-Alpiste, M.J., 2018. Zircon and apatite-bearing pyroxene hornblendite mantle xenolith from Hungary, Carpathian-Pannonian region. Lithos, 316, 19-32.

Bhowmik, S.K., Ao, A., 2016. Subduction initiation in the Neo-Tethys: Constraints from counterclockwise P–T paths in amphibolite rocks of the Nagaland Ophiolite Complex, India. Journal of Metamorphic Geology, 34(1), 7-44.

Blundy, J.D., Holland, T.J.B., 1990. Calcic amphibole equilibria and a new amphibole-plagioclase geothermometer. Contributions to Mineralogy and Petrology, 104, 208-224.

Buda, G.Y., 1993. Igneous petrology of the Bulfat area (north-east Iraqi Zagros thrust zone). Acta Mineralogica Petrographica, 34, 21-39.

Buday, T., Jassim, S.Z., 1987. The regional geology of Iraq, vol. 2: tectonism, magmatism and metamorphism. GEOSURV, Baghdad.

Cai, Y., Wang, Y., Cawood, P.A., Fan, W., Liu, H., Xing, X., Zhang, Y., 2014. Neoproterozoic subduction along the Ailaoshan zone, South China: Geochronological and geochemical evidence from amphibolite. Precambrian Research, 245, 13-28.

Christiansen, E.H., Hamblin, W.K., 2014. Dynamic Earth: an introduction to physical geology. Jones & Bartlett Publishers.

Colombi A., 1989. Métamorphisme et géochimie des roches mafiques des Alpes ouest-centrales (géoprofil Viége-Domodossola-Locarno). Mémoires de Géologie, 4, 1-216.

De Oliveira, D.P., Wiechowski, A., Robb, L.J., Inverno, C.M.C., 2003. Amphibolite vs. Banded Amphibolite: A Case Study in the São Martinho-Arronches Area, Tomar Cordoba Shear Zone, NE Ossa Morena Zone, Portugal. Cadernos Lab. Xeolóxico de Laxe Coruña, 28, 213-229.

Deer, W.A., Howie, R.A., Zussman, J., 1963. Rock-forming minerals: Framework silicates. Longmans, London

Demange, M.A., 2012, Mineralogy for Petrologists: Optics, Chemistry, and Occurrences of Rock-Forming Minerals: London, CRC Press.

Downes, H., Beard, A., Hinton, R., 2004. Natural experimental charges: an ion-microprobe study of trace element distribution coefficients in glass-rich hornblendite and clinopyroxenite xenoliths. Lithos, *75*(1-2), 1-17.

Drummond, D.A., Cloutier, J., Boyce, A.J., Prave, A.R., 2020. Petrogenesis and geochemical halos of the amphibolite facies, Lower Proterozoic, Kerry Road volcanogenic massive sulfide deposit, Loch Maree Group, Gairloch, NW Scotland. Ore Geology Reviews, 124, 103623.

Ernst, W.G., Liu, J., 1998. Experimental phase-equilibrium study of Al- and Ti-contents of calcic amphibole in MORB; a semiquantitative thermobarometer. American Mineralogist, 83 (9-10), 952–969.

Fanka, A., Tsunogae, T., Daorerk, V., Tsutsumi, Y., Takamura, Y., Endo, T. and Sutthirat, C., 2016. Petrochemistry and mineral chemistry of Late Permian hornblendite and hornblende gabbro from the Wang Nam Khiao area, Nakhon Ratchasima, Thailand: indication of Palaeo-Tethyan subduction. Journal of Asian Earth Sciences, 130, 239-255.

Fouad, S.F., 2015. Tectonic map of Iraq, scale 1: 1000 000, 2012. Iraqi Bulletin of Geology and Mining, 11(1),1-7.

Frisch, W., Meschede, M., Blakey, R.C., 2011. Plate Tectonics: Continental Drift and Mountain Building. Springer, 1–207.

Gill, R., and Fitton, G., 2022. Igneous rocks and processes: a practical guide. John Wiley & Sons.

Hadi, A., Kameran, D., Ismael, S., 2013. Characteristic of the Amphibolite Rocks of Penjween area, Kurdistan Region, Northeastern Iraq: Genetic implication and association with Penjween Ophiolite Complexes. Journal of Environment and Earth Sciences, 3, 14, 22-44.

Hamasalh, F.R., 2004. Petrochemistry, petrogenesis and tectonic setting of the Pauza Ultramafic rocks, Bulfat Complex, Northeast Iraq, Kurdistan region (Doctoral dissertation, MSc. Thesis, University of Sulaimani.

Hassan, D.K. and Ridha, A.P.A.H., 2018. Petrography and Mineralogy of Amphibolite Rocks in Penjween Complex, Northeastern Iraq. International Journal of Advanced Engineering Research and Science, 5(2), 237389.

Hollocher, K., Robinson, P., Walsh, E., Roberts, D., 2012. Geochemistry of amphibolite-facies volcanics and gabbros of the Støren Nappe in extensions west and southwest of Trondheim, Western Gneiss Region, Norway: a key to correlations and paleotectonic settings. American Journal of Science, 312(4), 357-416.

Jassim, S.Z., Waldhausrova J., Suk M., 1982a. Evolution of magmatic activity in Iraqi Zagros complexes. Krystalinikum, 16, 87-108.

Jassim, S.Z., Buda G., Neuzilova M., Suk M., 1982b. Metamorphic development of the Iraqi Zagros Ophiolite Zone. Krystalinikum, 16, 21-60.

Jassim, S.Z., Buday, T., Cicha, I., Opletal, M., 2006a. Tectonostratigraphy of the Zagros Suture. In: S.Z. Jassim & J.V. Goff (Eds.), Geology of Iraq. Brno, Czech Republic: Dolin, Prague and Moravian Museum. Chapter 16, pp 199-211.

Jassim, S.Z., Suk, M., Waldhausrova, J., 2006b. Magmatism and metamorphism in the Zagros Suture. In: S.Z. Jassim & J.V. Goff (Eds.), Geology of Iraq. Brno, Czech Republic: Dolin, Prague and Moravian Museum. Chapter 17, 212-231.

Karo, N.M., 2015. Metamorphic evolution of the Northern Zagros Suture Zone (NZSZ) (Doctoral dissertation, Universität Potsdam).

Karo, N.M., Oberhänsli, R., Aqrawi, A.M., Elias, E.M., Aswad, K.J., Sudo, M., 2018. New $^{40}Ar/^{39}Ar$ age constraints on cooling and unroofing history of the metamorphic host rocks (and igneous intrusion associates) from the Bulfat Complex (Bulfat area), NE-Iraq. Arabian Journal of Geosciences 11, 234.

Kettanah, Y.A., Ismail, S.A., Karo, N.M., 2022. Mineralogy, geochemistry, and $^{40}Ar/^{39}Ar$ dating of hornblendite/amphibolite pods in Penjween Ophiolite of northeastern Iraq: Implications for petrogenesis and tectonics. Journal of African Earth Sciences, 104591.

Kocak, K., Kurt, H., Zedef, V., Ferre, E.C., 2007. Characteristics of the amphibolites from Nigde metamorphics (Central Turkey), deduced from whole rock and mineral chemistry. Geochemical Journal, 41(4), 241-257.

Leake, B.E., Woolley, A.R., Arps, C.E.S., Birch, W.D., Gilbert, M.C., Grice, J.D., Hawthorne, F.C., Kato A., Kisch, H.J., Krivovichev, V.G., Linthout, K., Laird, J., Mandarino, J.A., Maresch, W.V., Nickel, E.H., Rock N. M. S., Schumacher J. C., Smith D. C., Stephenson N. C. N., Ungaretti L., Whittaker E. J. W., Youzhi G., 1997. Nomenclature of amphiboles: Report of the sub-committee on amphiboles of the international mineralogical association. Commission on new minerals and mineral names. American Mineralogist, 82, 1019-1037.

Ma, X., Fan, H.R., Santosh, M., Guo, J., 2016. Petrology and geochemistry of the Guyang hornblendite complex in the Yinshan block, North China Craton: Implications for the melting of subduction-modified mantle. Precambrian research, 273, 38-52.

Mendes, J.C., Ghizi, A., Junho, M.D.C.B., 2004. Diorite and hornblendite enclaves at sumidouro, RJ, Central Ribeira Belt. Brazilian Journal of Geology, 34(1),79-86.

Mohajjel, M., Fergusson, C.L., Sahandi, M.R., 2003. Cretaceous–Tertiary convergence and continental collision, Sanandaj–Sirjan zone, western Iran. Journal of Asian Earth Sciences, 21(4),397-412.

Morimoto, N., 1988. Nomenclature of pyroxenes. Mineralogy and Petrology, 39(1),55-76.

Nesse, W.D., 2000. Introduction to Mineralogy. New York, Oxford: Oxford University Press.

Otten, M.T., 1986. The origin of brown hornblende in the Artfjället gabbro and dolerites. Contributions to Mineralogy and Petrology, 86(2), 189-199.

Pearce, T.H., Gorman, B.E., Birkett, T.C., 1977. The relationship between major element chemistry and tectonic environment of basic and intermediate volcanic rocks. Earth and Planetary Science Letters, 36(1), 121-132.

Polat, A., Fryer, B.J., Samson, I.M., Weisener, C., Appel, P.W., Frei, R., Windley, B.F., 2012. Geochemistry of ultramafic rocks and hornblendite veins in the Fiskenæsset layered anorthosite complex, SW Greenland: Evidence for hydrous upper mantle in the Archean. Precambrian Research, 214,124-153.

Sadegh, H.R., Moeinzadeh, H., Moazzen, M., 2021. Geochemistry and geochronology of amphibolites from the Sirjan area, Sanandaj-Sirjan zone of Iran: Jurassic metamorphism prior to Arabia and Eurasia collision. Journal of Geodynamics, 143,101786.

Santana, L.V., McLeod, C.L., Blakemore, D., Shaulis, B., Hill, T., 2020. Bolivian hornblendite cumulates: Insights into the depths of Central Andean arc magmatic systems. Lithos. 370,105618.

Schmidt, M.W., 1992. Amphibole composition in tonalite as a function of pressure: an experimental calibration of the Al-in-hornblende barometer. Contributions to mineralogy and petrology, 110, 304-310.

Schumacher, J.C., Smith, D.C., Stephenson, N.C.N., Ungaretti, L., Whittaker, E.J.W., Youzhi G., 1997. Nomenclature of amphiboles: Report of the sub-committee on amphiboles of the international mineralogical association. Commission on new minerals and mineral names. American Mineralogist, 82, 1019-1037.

Sheikhi, F., Razavi, S.M.H., Alaminia, Z., Lotfi, M., 2020. Geothermobarometry of Amphiboles in Granitoid Rocks From the Baghche Maryam Area, Sanandaj-Sirjan Zone, NW Iran. Revista Geoaraguaia, 10, 108-129.

Sun, S.S., McDonough, W.F., 1989. Chemical and isotopic systematics of oceanic basalts: implications for mantle composition and processes. Geological Society, London, Special Publications, 42(1),313-345.

Sun, S.S., Bailey, D.K., Tarney, J.,Dunham, K., 1980. Lead isotopic study of young volcanic rocks from mid-ocean ridges, ocean islands and island arcs. Philos Trans R Soc London A297, 409-445

Torabi, G., Arai, S., Morishita, T.,Tamura, A., 2017. Mantle hornblendites of Naein ophiolite (Central Iran): Evidence of deep high temperature hydrothermal metasomatism in an upper mantle section. Petrology, 25(1), 114-137.

Wang, W.L., Aitchison, J.C., Lo, C.H. and Zeng, Q.G., 2008. Geochemistry and geochronology of the amphibolite blocks in ophiolitic mélanges along Bangong-Nujiang suture, central Tibet. Journal of Asian Earth Sciences, 33(1-2), 122-138.

Wilson, J.R., 2010. Minerals and rocks. Bookboon

Winter J.D, 2010. An introduction to igneous and metamorphic petrology. Prentice Hall, New Jersey.